Fractography, elastic modulus, and oxidation resistance of Novel metal–intermetallic Ni/Ni_3Al multilayer films

X.K. Meng,[a] H. Shen, and H. Vehoff
Institute of Materials Science and Methods, University of Saarland, 66041 Saarbrücken, Germany, and National Laboratory of Solid State Microstructures, Nanjing University, Nanjing 210093, People's Republic of China

S. Mathur
Institute of Inorganic Chemistry, University of Saarland, 66041 Saarbrücken, Germany

A.H.W. Ngan
Department of Mechanical Engineering, University of Hong Kong, Pokfulam Road, Hong Kong

(Received 18 May 2001; accepted 22 January 2002)

Novel metal–intermetallic Ni/Ni_3Al multilayer films are synthesized by a magnetron sputtering technique. The fractography, elastic modulus, and the oxidation resistance of the multilayer films are studied by a series of experimental tests. The scanning electron microscopy fractography of the films shows that both Ni and Ni_3Al layers fracture with the appearance of ductile metal failure. No metal–intermetallic delamination appears in the multilayered films. Fluted dimpling in each Ni and Ni_3Al layer is evident and continuous, layer through layer, illustrating very good adherence among the constituent layers. Such adherence makes the toughness of the Ni layers capable of transferring into the Ni_3Al layers. Young's modulus of the Ni/Ni_3Al film is found to be 226 and 253 ± 10 GPa by nanoindentation and laser acoustic techniques, respectively. The continuity of elastic modulus between the two phases is revealed by nanoindentation test. The modulus continuity indicates an excellent integration of the constituent layers with similar crystal structure and close lattice constants. This integration makes the multilayers unsurpassed in comprehensive mechanical properties. Sheet resistance measurements show a good protective ability of the Ni/Ni_3Al multilayers during high temperature oxidation. X-ray photoelectron spectroscopy spectra suggest that crystallized Al_2O_3/Ni scales formed during the deposition and subsequent annealing processes are apparently responsible for the stability of these films under oxidative conditions. The appearance of the crystallized Al_2O_3/Ni thin scales on the top of Ni_3Al layers provides the Ni/Ni_3Al multilayers good thermal oxidation resistance without lowering the fracture toughness.

I. INTRODUCTION

Multilayers synthesized from constituents having similar structures and a modest lattice mismatch often exhibit grain-to-grain epitaxy between the layers even in case the gross structure is polycrystalline.[1] When the constituent layers are chosen appropriately, good atomic coherence and hence good inherent properties of the individual constituents may be inherited by the multilayers.

Nickel is used as the basis or as a major component of numerous alloys for high-temperature application.[2] It is of particular industrial interest because of its satisfied resistance to corrosion and excellent ductility under mechanical loading.[3] Intermetallic Ni_3Al both in bulk and thin-film state possesses a number of desirable properties such as high fracture toughness and high oxidation resistance at elevated temperatures.[4,5] Although high ductility and even low-temperature superplasticity of specially processed Ni_3Al alloys have been reported recently and some of them have found applications in high-temperature furnaces,[6–8] the practical use of the intermetallics is still limited by room-temperature brittleness and poor high-temperature creep resistance.

It is noteworthy that nickel and Ni_3Al have not only similar structures but also close unit cell dimensions. Nickel is a face-centered-cubic (fcc) structured metal with a lattice constant of 0.3524 nm, while Ni_3Al possesses an ordered fcc $L1_2$ structure with aluminum atoms occupying alternative sites on every other (111) plane.

[a]Permanent address: National Lab. of Solid State Microstructures, Nanjing University, Nanjing 210093, P.R. China.
e-mail: mengxk@yahoo.com

The lattice constant of Ni_3Al is 0.3570 nm, which is only 1.29% larger than that of nickel. In this context, incorporating nickel with intermetallic Ni_3Al might produce grain-to-grain epitaxial interfaces. Recent x-ray diffraction (XRD) measurements revealed the high vertical coherence over several bilayers of Ni and Ni_3Al thickness.[9–11] The highly coherent interfaces were thought to play important role in overcoming the intrinsic brittleness of most superalloyed Ni/Ni_3Al composites Ni_3Al alloys and, hence, make them unsurpassed by all other materials in special structural applications in which great strength, toughness, thermal and corrosion protection, and damage tolerance are required.[12–14]

Recently, we have reported some experimental results on the Ni/Ni_3Al multilayer film system.[15] The preliminary results on microlaminated Ni/Ni_3Al films suggested a potential application of these films as structural components because the Ni/Ni_3Al multilayers are both hard and ductile enough. In this paper, we report the fractography, elastic modulus, and oxidation resistance of the metal–intermetallic Ni/Ni_3Al multilayer films. Fractography is used to evaluate the ductility and toughness of these films. We are interested in knowing the elastic modulus of these films because a high elastic modulus is a key requirement for high-precision application.[16] It may also be essential for metal-based multilayers to have satisfactory oxidation resistance to be used durably in high-temperature environments.

II. EXPERIMENTAL DETAILS

Ni/Ni_3Al multilayer films were deposited on Si single crystals by a magnetron sputtering system. Two sputtering targets of Ni (99.95% pure) and Ni + Al (99.5% pure) for producing Ni and Ni_3Al layers, respectively, were fixed on opposite faces of the chamber, while the substrate is mounted on a block that could be rotated, if necessary. The Ni + Al target was prepared by cutting Al sheets into sectors with an angle of 10°, followed by gluing on a Ni disc, leaving alternate gaps to expose the Ni underneath. The base pressure before sputtering was controlled at 1×10^{-5} torr, and the chamber pressure maintained at 5×10^{-2} torr during sputtering with argon ions. The substrate temperature was kept at 400 °C to increase the surface mobility of atoms, leading to enhanced crystallization of the thin films.[17] Multilayered samples were prepared this way with equal Ni and Ni_3Al layer thickness, which ranged between 35 and 1000 nm in size. The number of the constituent layers ranged between 4 and 30 in total.

The as-deposited multilayers were annealed at 700 °C to enable the constituent layers to crystallize. Microstructure features were characterized using scanning electronic microscopy (SEM) combined with energy-dispersive x-ray spectroscopy (EDXS), as well as transmission electronic microscopy (TEM). Collodion technique was employed for TEM sample preparation. (Standard openwork of copper foil was coated with collodion and then used as a sputter substrate.) To characterize the toughness of the multilayers, a four-point bending method is introduced to break the samples of multilayer on silicon substrate. By this way the cross section is fractured smoothly and the SEM fractograph is imaged with satisfied quality.

Nanoindentation and laser-acoustic techniques were applied to measure the elastic modulus of the multilayers. Nanoindentation allows quantitative and ultralocalized (at the nanometer scale) measurements of hardness and indent modulus by analyzing the accurate load–displacement data recorded by an additional PC during testing. Although it cannot produce a rigorous measurement of Young's modulus, derivative methods developed by Doerner and Nix[18] and Oliver and Pharr[19] provide a practical evaluation of elastic modulus from the unloading curves of indentation for homogeneous and isotropic materials. Since the multilayered films are intrinsically anisotropic, the modulus obtained is only useful as relative values.[20] Some other methods, e.g., the laser-acoustic technique, will be compensative to determine Young's modulus of the multilayered thin films. The laser-acoustic technique relates to an approach of an effective medium of transversal symmetry to describe the elastic anisotropy of the multilayer films. It treats the multilayers as a single film of transversal symmetry that is only governed by six equations of boundary conditions.[21,22] The averaged Young's modulus of multilayers can be calculated from the measured values of phase velocity c under a series of circular frequency ω. This way is useful if there is not any other information available for a multilayer film.

The as-annealed samples were reannealed respectively at temperatures of 800, 900, and 1000 °C in air for 30 min to study the oxidation resistance and thermal stability of the Ni/Ni_3Al multilayers. The sheet resistance of the samples was measured by a four-point probe. X-ray photoelectron spectroscopy (XPS) analysis was carried out in an SSI (Surface Science Instruments, CA) spectrometer with a hemispherical electron energy analyzer using A1 K_α irradiation with an energy resolution of 0.8 eV. The binding energy resolution of the spectroscope is approximately ±0.05 eV. All the samples were presputtered at 500 eV for 1 min before normal testing to remove the surface contamination. For comparison sake, bulk Ni_3Al polycrystalline was also analyzed.

III. EXPERIMENTAL RESULTS

Composition analysis by EDXS shows that the Ni:Al atomic ratio in the as-deposited Ni–Al layers is close to 3:1 when a Ni + Al target with 13 sectors of Al on Ni disc

is used in the sputtering process. This Ni + Al target is therefore convenient to produce Ni_3Al layers in the multilayer films. XRD analysis demonstrates that the as-deposited Ni–Al layer was a whole Ni_3Al phase if the layer was annealed at 700 °C for 1 h.[15]

An SEM cross section of a 30-layer Ni/Ni_3Al film and TEM surface image of an annealed 2-layer Ni/Ni_3Al film are shown in Figs. 1(a) and 1(b), respectively. The individual layer thickness is approximately 35 nm, as shown in Fig. 1(a). A selected area diffraction pattern from the multilayer is also shown at the bottom left corner of Fig. 1(b). The rings marked as r_1 and r_4 in Fig. 1(b) are superlattice reflections resulting from the ordered Ni_3Al.

The SEM fractographs of as-deposited and as-annealed multilayers with 4 alternate layers of Ni and Ni_3Al are shown in Figs. 2(a) and 2(b), respectively. The

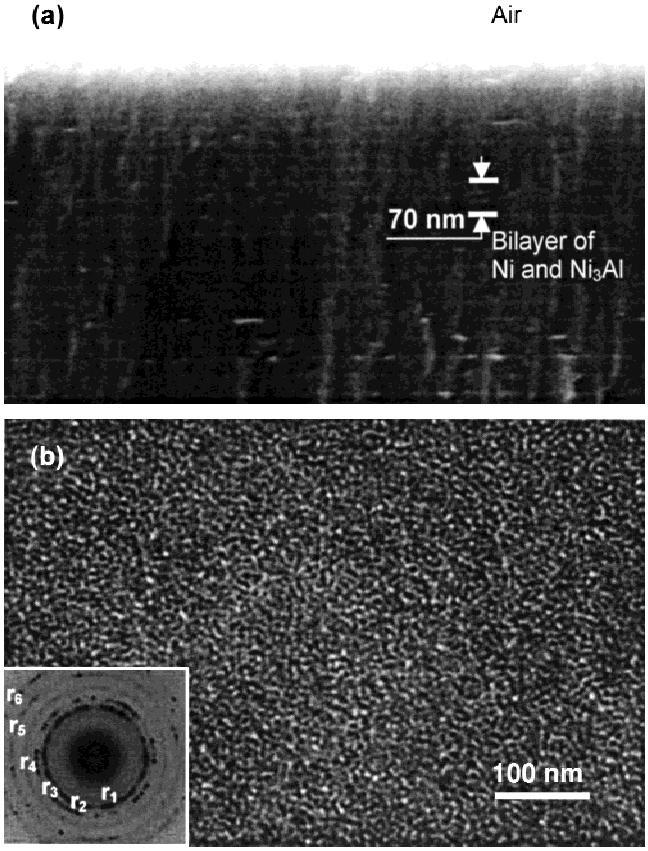

FIG. 1. (a) SEM cross section of a 30-layer Ni/Ni_3Al film and (b) TEM surface images of a 2-layer Ni/Ni_3Al film multilayer. The two multilayers are synthesized and annealed at the same conditions. The individual layer thickness is approximately 35 nm. The electron diffraction pattern at the bottom left corner of (b) includes overlapped rings from both Ni and Ni_3Al polycrystals, marked as r_2, r_3, r_5, and r_6, which corresponded to diffraction faces of (111), (200), (220), and (400), respectively. The rings marked as r_1 and r_4 resulted only from diffraction faces of (110) and (210) in Ni_3Al, respectively. The TEM surface image shows the structure is polycrystalline with grains in nanometer size.

samples for better fractograph purpose are synthesized with relatively thick individuals, each approximately 900 nm in layer thickness.

The nanoindentation result of the same multilayer is shown in Fig. 3(a). The values of indentation modulus vary from 218 to 285 GPa in an indent depth range between 208 and 1317 nm. The fitted curve shows that the modulus stays almost at a constant value of 226 GPa when the indentation depth is larger than 412 nm. The measured c–ω curve of a multilayer consisting of 8 alternative layers of Ni and Ni_3Al with individual layer thickness of approximately 900 nm is shown in Fig. 3(b). The dispersion curve is fitted with a theoretical curve to obtain the layer parameters by using the well-known least-squares method. The fit procedure results in a Young's modulus of $E = 253 \pm 10$ GPa for the Ni/Ni_3Al multilayer film.

Table I shows the variation of the sheet resistance of the as-deposited, as-annealed, and reannealed multilayers. The samples consist of 6 individual layers, with each approximately 120 nm in thickness. The sheet resistance stays nearly constant at approximately 30 Ω/sq during reannealing from 800 to 1000 °C in air. The XPS spectra of the multilayer system and a standard sample of bulk Ni_3Al alloy (for comparison) are shown in Fig. 4. Figure 4(a) shows the overview XPS spectrum of the as-deposited and annealed multilayers. Figure 4(b) relates to the Ni 2*p* spectra, while Ni 3*p* and Al 2*p* XPS spectra are exhibited in Fig. 4(c).

IV. DISCUSSION

A. Fractography of the multilayers

As mentioned above, the similar structure and small lattice mismatch of Ni and Ni_3Al are expected to result in grain-to-grain epitaxial Ni/Ni_3Al interfaces, and hence, the grain boundary brittleness of Ni_3Al should be overcome effectively. (The conventional TEM investigations cannot prove this because the grain size within a layer is too small to enable the grain boundaries to be seen clearly.) In such a case, Ni/Ni_3Al multilayers should possess satisfactory ductility and fracture strength.

It is intriguing to find that the bending fractographs of the Ni/Ni_3Al multilayers shown in Fig. 4 indeed demonstrate such an expectation. Both the Ni and Ni_3Al layers fracture with the appearance of ductile metal failure. Intermetallic Ni_3Al layers fracture by fluted dimpling rather than brittle cleavage. No metal–intermetallic delamination appears in the multilayered film. The fluted dimpling in the completely crystallized multilayer is more evident and continuous, layer through layer, illustrating the good adherence of Ni and Ni_3Al layers. Such adherence makes the toughness of the Ni layers able to transfer into Ni_3Al layer. This differs from the interruption of toughness observed in some

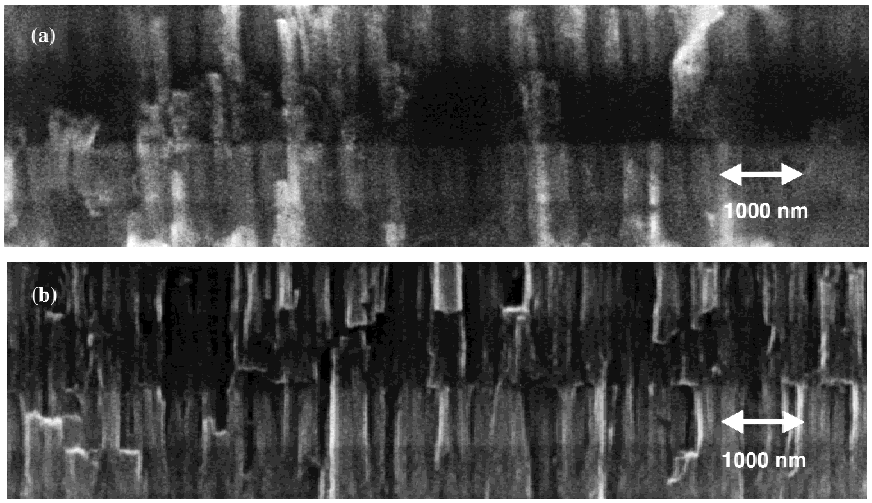

FIG. 2. Fractographs of (a) as-deposited and (b) as-annealed multilayers with 4 alternate layers of Ni and Ni_3Al. The total thickness of the multilayers is approximately 3600 nm, with individual thickness of constituents 900 nm in size.

other metal–intermetallic multilayer thin films. For example, in bcc/A15-structured Nb/Nb_3Al (a_{Nb} = 0.330 nm, a_{Nb_3Al} = 0.519 nm) and bcc/C15-structured Nb(Cr)/Cr_2Nb (a_{Nb} = 0.330 nm, a_{Cr} = 0.288 nm, a_{Cr_2Nb} = 0.699 nm) multilayer thin films,[23,24] metallic Nb and Nb(Cr) layers fractured with the appearance of ductile failure while intermetallic Nb_3Al and Cr_2Nb layers failed by brittle and flat cleavage. The interruption of fluted dimpling between metallic and intermetallic layers indicates a failure in building a tough multilayered thin film. This failure may be attributed mainly to the large deference in their unit cell dimensions. Such a difference makes it very difficult to form atomic coherent interfaces between layers, and hence, the intermetallic layers preserve their intrinsic character of brittle failure mode. Unlike the brittle Nb_3Al and Cr_2Nb layers, the Ni_3Al layer in our Ni/Ni_3Al system shows the transformation of toughness from its intrinsic brittleness by combining with metal layers of Ni whose crystal structure and lattice constant are very close to the former.

B. Elastic modulus of the multilayers

The determination of Young's modulus of materials is most useful for any design application in microelectromechanical systems. Generally speaking, Young's modulus of a given metal or alloy is related to the bonding forces between the atoms concerned to an applied stress. It determines the residual stresses as well as elastic energy induced by external loading, which is responsible for initiating cracks and microfractures.[25] From this point of view, different structures should have different elastic properties and, hence, discontinuities of elastic modulus should appear at structural transformations.

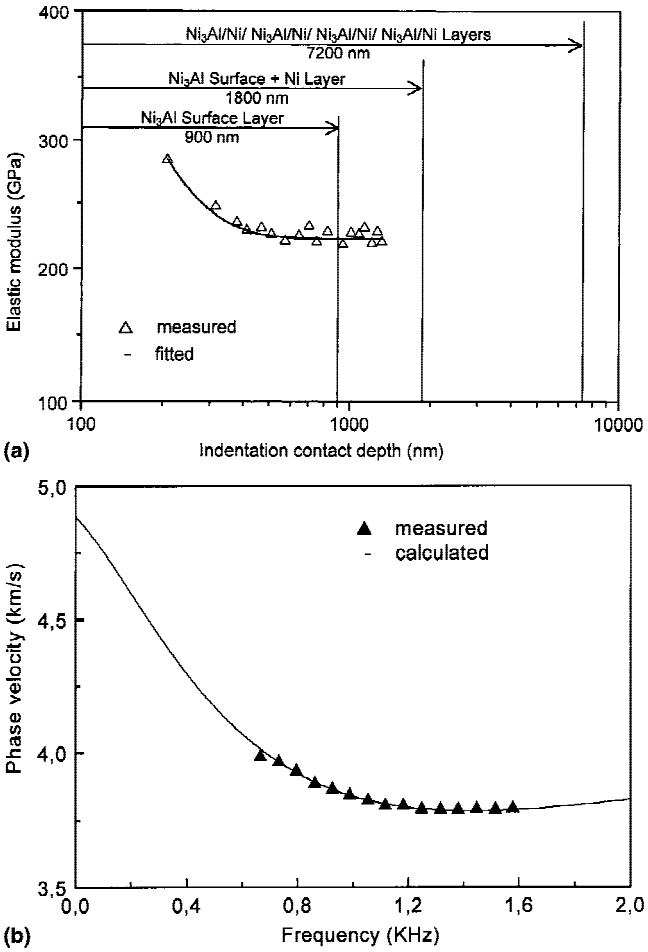

FIG. 3. Plots of (a) indentation modulus as a function of contact depth and (b) phase velocity as a function of frequency. The multilayer consists of 8 alternative layers of Ni and Ni_3Al with an individual layer thickness of approximately 900 nm. The topmost layer is deposited as Ni_3Al.

TABLE I. Sheet resistance of multilayer samples at various temperatures. The samples consist of 6 individual layers, with each approximately 120 nm in thickness.

	As-deposited samples[a]	As-annealed samples[b]	Reannealed samples (in air for 30 min)		
Reannealing temperature (°C)	···	···	800	900	1000
Sheet resistance (Ω/sq)	1100	21	28	25	32

[a]400 °C in argon.
[b]700 °C in vacuum for 60 min.

The modulus measured by the nanoindentation technique increases significantly with decreasing indentation depth when the depth is below 208 nm. The decrease in modulus would appear to be directly related to the probing of the hard Ni_3Al top layer. That is to say, the modulus of the Ni_3Al film synthesized is larger than the value of 226 MPa, which is almost twice that reported by Huang *et al.*,[5] as can be seen from the fitted curve in Fig. 3(a). It should be noted that the maximum indentation contact depth does not exceed 1320 nm, which is within 20% of the total film thickness of 7200 nm, and hence, the measured modulus should be free from substrate effects.[26,27] In this case, substrate-induced enhancement of pile-up is negligible, and the modulus values measured by nanoindentation techniques are within 10% of the expected values.[28] Therefore, the value of 226 GPa can be regarded as an indentation-resulted modulus. It is very close to the result of 253 ± 10 GPa obtained by the laser-acoustic technique, as shown in Fig. 3(b). Therefore, Young's modulus of the present multilayer film should be at the value of 230–250 MPa. It is only a bit small than a newly reported result on nanolaminated multilayers, which ranges from 256.2 to 288.5 GPa.[11]

Except the initial data resulting from the probing of the hard Ni_3Al top layer, Young's modulus values do not change significantly with contact depth, even when the indenter tip penetrates from one layer to another. It exemplifies the continuity of elastic modulus between the two phases. The discontinuity of elastic modulus does not appear at Ni and Ni_3Al structural transformation, meaning all layers have the same texture, as revealed by XRD.[10] The modulus continuity indicates an excellent integration of the constituent layers with similar crystal structures and close lattice constants. This integration makes the multilayers unsurpassed in comprehensive mechanical properties.

C. Oxidation resistance of the multilayers

The sheet resistance of the as-deposited multilayer film is rather large (up to 1100 Ω/sq), as shown in Table I. This large resistance mainly results from the

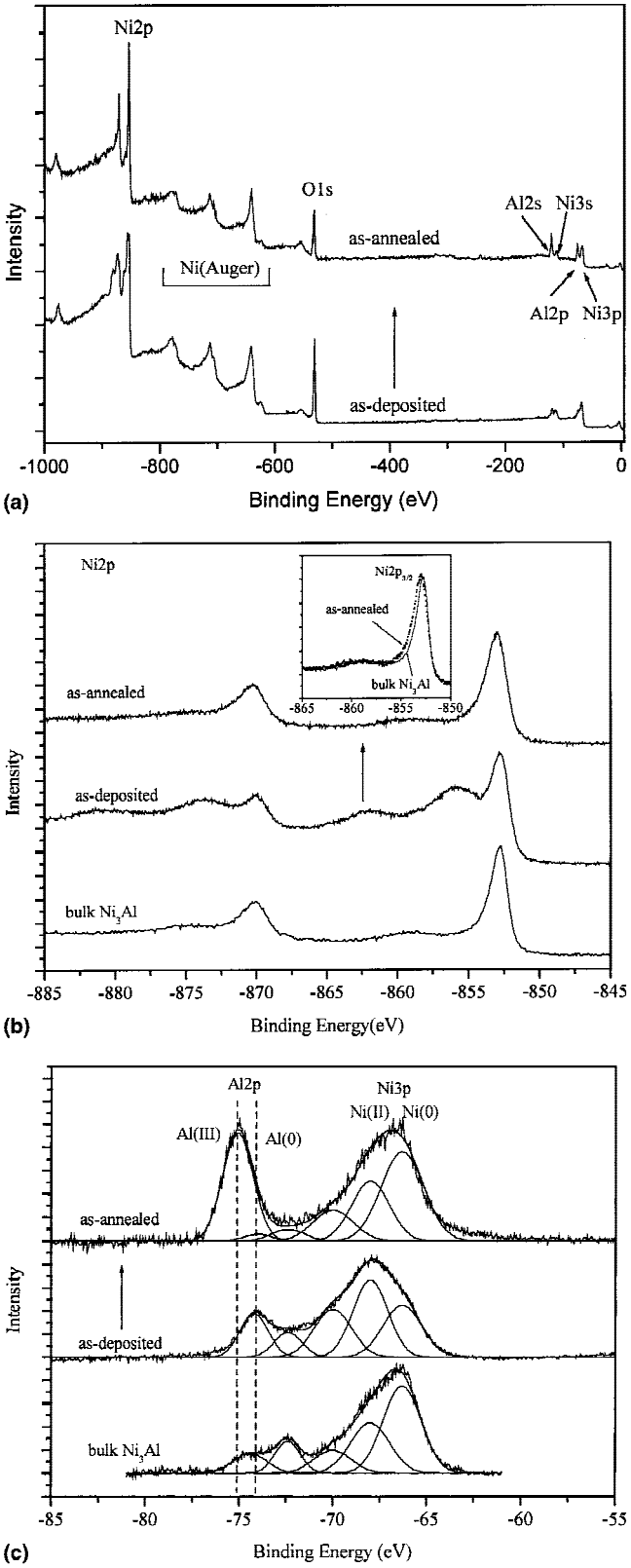

FIG. 4. (a) Overview XPS spectra of as-deposited and annealed Ni–Al films (in vacuum at 690 °C), (b) Ni 2*p* XPS spectra of as-deposited and annealed Ni–Al thin films and a bulk Ni_3Al alloy, and (c) Ni 3*p* and Al 2*p* XPS spectra of as-deposited and annealed Ni–Al thin films and a bulk Ni_3Al alloy.

partial ordering or crystallization of the surface layer of Ni–Al film. After completely crystallization at 700 °C, the sheet resistance of the multilayer lowers dramatically to approximately 30 Ω/sq and remains almost constant during the subsequent reannealing steps at high temperature in air. This result shows the very good protective ability of the Ni/Ni_3Al multilayers during high-temperature oxidation conditions.

The XPS spectra shown in Fig. 4 reveal that the high-temperature stability as shown is attributed to the formation of crystallized Al_2O_3/Ni thin scales on the top of Ni/Ni_3Al multilayers. The O 1*s* peak detected in the as-deposited multilayer in Fig. 4(a) shows that the oxide scale originates from the deposition process. Although the sputtering chamber was vacuumed and filled with argon gas before deposition process, some residual oxygen would inevitably remain and may result in the oxidation of a part of the constituent atoms of sputtered Ni and Al. The Ni 2*p* peak in Fig. 4(b) and A1 2*p* peak in Fig. 4(c) demonstrate the existence of Ni and Al oxides, respectively.

The atomic ratios of Ni to Al on the surface of bulk Ni_3Al, the as-deposited multilayers, and the as-annealed multilayers are approximately 3:1, 3:1, and 1:1, respectively, as can be found by calculating the intensity area and cross section of the related A1 2*p* and Ni 3*p* peaks from Fig. 4(c). The change of element contents and evolution of phases are revealed clearly by comparing with the XPS spectra recorded before and after annealing. The metallic Al (with binding energy of −72 eV) and Al oxide (with binding energy of −74 eV) in the as-deposited multilayers diffuse outward and aggregate on the surface when annealing is performed at high temperature, resulting in an increased content of Al on the surface. The Al oxide in the as-deposited state is assumed to be amorphous because of its relative lower binding energy of −74 eV. After annealing, the Al 2*p* peak is shifted to a higher value of −75 eV, which means that the amorphous Al oxide is crystallized at high temperatures. No metallic A1 2*p* peak appears in the as-annealed sample anymore, indicating that the metallic Al is oxidized during annealing, even under vacuum conditions. This is in contrast with Ni oxide formed during depositing process. Only Ni 2*p* and Ni 3*p* peaks from metallic Ni (note the lower binding energy) can be detected in the as-annealed sample, illustrating that the Ni oxide formed during deposition [see the double peaks located at −855 and −863 eV in Fig. 4(b)] is reduced after annealing. As shown in the inset in Fig. 4(b), the line of the Ni $2p_{3/2}$ peak in the as-annealed sample is more broadened and asymmetric than that observed in bulk Ni_3Al. This demonstrates further the reduction of Ni oxide, leading to the formation of metallic Ni on the surface of the multilayer, because it is well known that the broadening of the Ni $2p_{3/2}$ main line increases with decreasing aluminum content in Ni–Al alloys.[29] The oxygen eliminated during the reduction of Ni oxide provides oxidative condition for the newly arrived Al on the surface of the multilayer. Consequently, the metallic Al peak disappears in the as-annealed samples even when the annealing has performed in vacuum. The redox reaction of the Ni oxide and Al is explainable as

$$3\mathrm{NiO} + 2\mathrm{Al} \xrightarrow[\text{vacuum}]{\Delta} \mathrm{Al_2O_3} + 3\mathrm{Ni} \quad .$$

It indicates that the annealing is not only responsible for the crystallization of Ni_3Al layers but also for the formation of Al_2O_3/Ni surface scales on the top Ni_3Al layers. Zalar *et al.*[30] studied a different system of Ni/Al multilayers and found the formation of Ni_3Al and $NiAl_3$ phases with excess of Ni in the annealed Ni_3Al samples. They found a thicker oxide film on the top of the annealed Ni_3Al layer, which consists of NiO on the top and some Al_2O_3 below. In our Ni/Ni_3Al system, NiO is completely reduced during the annealing of the multilayers. Surface scales of Al_2O_3/Ni rather than Al_2O_3/NiO are formed on the top of Ni_3Al layers. Al_2O_3 is chemically stable and mechanically strong, possessing very good protective ability at high temperature.[31] By mixing of the material with some other metallic elements like Ni or Cu, its mechanical properties can be further enhanced, especially in hardness and toughness.[32,33] On this account, the appearance of the crystallized Al_2O_3/Ni thin scales on the top of Ni_3Al layers provides the Ni/Ni_3Al multilayers good thermal oxidation resistance without lowering the fracture toughness.

V. CONCLUDING REMARKS

Multilayers synthesized from constituents with similar structures and modest lattice mismatch are expected to produce good atomic coherence between the constituent layers and hence inherit the good mechanical properties of the constituents. Metallic Ni and intermetallic Ni_3Al have similar structures and close unit cell dimensions. The good mechanical properties such as high flow stress[13] and fracture toughness[34,35] in Ni-based superalloys are usually attributed to the contribution of coherent interfaces between γ–Ni matrix and γ′–Ni_3Al (or some other like Ir_3Nb) precipitates. This stimulated us to develop a novel type of Ni/Ni_3Al multilayer films which possess complementary mechanical properties for application as mechanical elements in developing area.

The synthesis of the Ni/Ni_3Al multilayer films by means of magnetron sputter is quite simple if an appropriate target for producing Ni_3Al layer is prepared. The partial oxidation of Al and Ni atoms by rest gases during the deposition process permits the formation of thin

Al_2O_3/Ni protective scales on the surface of the multilayers. In mechanical aspects, the fracture toughness and Young's modulus of the Ni/Ni_3Al multilayers are quite satisfactory, although further characterization for the former (except for fractography) is to be done. The study of interface between Ni and Ni_3Al layers is also an important work in the next step, to clarify whether the coherent Ni/Ni_3Al interfaces play a key role in improving the mechanical properties of the multilayer films.

ACKNOWLEDGMENTS

We gratefully acknowledge K.L. Wang, M. Kempf, and M. Jillavi for assistance on sample preparing and experimental testing. X.K.M. and S.M. acknowledge in particular the Alexander von Humboldt Foundation of Germany for research fellowship. This work is financially sponsored by the Natural Science Foundation of China under Contract No. 59981003.

REFERENCES

1. B.M. Clemens, H. Kung, and S.A. Barnett, MRS Bull. **24**(2), 20 (1999).
2. A.M. Huntz, B. Lefevre, and F. Cassino, Mater. Sci. Eng. A **290,** 190 (2000).
3. W. Betteridge, in *Nickel and its Alloys* (Macdonald and Evans, Estover, United Kingdom, 1977), p. 124.
4. H.P. Ng, X.K. Meng, and A.H.W. Ngan, Scr. Mater. **39,** 1737 (1998).
5. Y. Huang, J. Aziz, J.W. Hutchinson, A.G. Evans, R. Saha, and W.D. Nix, Acta Mater. **49,** 2853 (2001).
6. T. Hirano, *Fracture Strength of Grain Boundaries in Ni_3Al,* presented at the University of Saarland, Saarbrücken, Germany, Dec. 8, 2000.
7. S.X. McFadden, R.S. Mishra, R.Z. Valiev, A.P. Zhilyaev, and A.K. Mukherjee, Nature **398,** 684 (1999).
8. M. Yamaguchi, H. Inui, and K. Ito, Acta Mater. **48,** 307 (2000).
9. H. Van Swygenhoven, H. Grimmer, F. Paschoud, M. Victoria, and R. Hauert, Nanostruct. Mater. **4,** 409 (1994).
10. S. Tixie, P. Böni, and H. Van Swygenhoven, J. Vac. Sci. Technol., A **16,** 2429 (1998).
11. S. Tixie, P. Böni, and H. Van Swygenhoven, Thin Solid Films **342,** 188 (1999).
12. Y. Yamabe-Mitarai, Y. Ro, T. Maruko, and H. Harada, Metall. Mater. Trans. A **29,** 537 (1998).
13. X.H. Yu, Y. Yamabe-Mitarai, and H. Harada, Scr. Mater. **43,** 671 (2000).
14. Y. Liu, K.Y. Chen, K. Lu, J.H. Zhang, and Z.Q. Hu, Acta Mater. **45,** 1837 (1997).
15. X.K. Meng, H. Vehoff, and A.H.W. Ngan, J. Mater. Res. **15,** 2595 (2000).
16. S.M. Spearing, Acta Mater. **48,** 179 (2000).
17. H. Chuang, M.H. Jilavi, T.P. Duffey, J. Mazumder, and W.M. Kriven, Scr. Mater. **38,** 429 (1998).
18. M.F. Doerner and W.D. Nix, J. Mater. Res. **1,** 601 (1986).
19. W.C. Oliver and G.M. Pharr, J. Mater. Res. **7,** 1564 (1992).
20. J.A. Ruud, T.R. Jervis, and F. Spaepen, J. Appl. Phys. **75,** 4969 (1994).
21. D. Grimsditch, Phys. Rev. B **31,** 6818 (1985).
22. D. Schneider, B. Schultrich, H.J. Scheibe, H. Ziegele, and M. Griepentrog, Thin Solid Films **332,** 157 (1998).
23. R.G. Rowe, D.W. Skelly, M. Larsen, J. Heathcote, G.R. Odette, and G.E. Lucas, Scr. Mater. **38,** 1487 (1994).
24. R.G. Rowe and D.W. Skelly, in *Intermetallic Matrix Composites II*, edited by D.B. Mriacle, D.L. Anton, and J.A. Graves. (Mater. Res. Soc. Symp. Proc. **273,** Pittsburgh, PA, 1992), p. 411.
25. D. Schneider and M.D. Tucker, Thin Solid Films **290–291,** 305 (1996).
26. Standard Test Method for Vicks Hardness of Metallic Materials (ASTM, West Conshohocken, PA, 1987).
27. T.Y. Tsui and G.M. Pharr, J. Mater. Res. **14,** 2204 (1999).
28. T.Y. Tsui and G.M. Pharr, J. Mater. Res. **14,** 292 (1999).
29. F.U. Hillebrecht, J.C. Fuggle, P.A. Bennet, Z. Zolnierek, and C. Freiburg, Phys. Rev. B **27,** 2179 (1983).
30. A. Zalar, S. Hofmann, D. Kohl, and P. Panjan, Thin Solid Films **270,** 341 (1995).
31. K. He, H. Gong, K. Zeng, Z. Li, and W. Gao, Mater. Lett. **46,** 53 (2000).
32. R.R. Oberle, M.R. Scanlon, R.C. Cammarata, and P.C. Searson, Appl. Phys. Lett. **66,** 19 (1995).
33. M. Besterci, J. Ivan, and L. Kovac, Mater. Lett. **46,** 181 (2000).
34. H.P. Xu, A.H.W. Ngan, and B.J. Duggan, Mater. Lett. **31,** 233 (1997).
35. W.H. Tian, T. Sano, and M. Nemoto, Scripta Metall. **20,** 933 (1986).